

# Spectroscopy and hydrodynamics of dense stellar winds

Wolf-Rainer Hamann\*, Götz Gräfener\*,<sup>†</sup>, Lidia M. Oskinova\* and Achim Feldmeier\*

\*Universität Potsdam, Germany  
<sup>†</sup>Armagh Observatory, Northern Ireland

**Abstract.** Analyzing the spectra from Wolf-Rayet stars requires adequate non-LTE modeling of their expanding atmosphere. The numerical schemes for solving the radiative transfer in the co-moving frame of reference have been developed by Mihalas and co-workers 30 years ago. The most elaborate codes can cope today with many hundred explicit non-LTE levels or super-levels and account for metal-line blanketing.

The limited agreement with observed spectra indicates that the model simplifications are still severe. One approximation that has to be blamed is homogeneity. Stellar-wind clumping on small scales was easily implemented, while "macro-clumping" is still a big challenge. First studies showed that macro-clumping can reduce the strength of predicted P-Cygni line profiles in O-star spectra, and largely affects the X-ray line spectra from stellar winds.

The classical model for radiation-driven winds by Castor, Abbot and Klein fails to explain the very dense winds from Wolf-Rayet stars. Only when we solved the detailed non-LTE radiative transfer consistently with the hydrodynamic equations, mass-loss rates above the single-scattering limit have been obtained.

**Keywords:** Radiative transfer, Mass loss, stellar winds, Wolf-Rayet stars

**PACS:** 95.30.Jx, 95.30.Lz, 97.10.Ex, 97.10.Fy, 97.10.Me, 97.30.Eh

## 1. MODELING THE SPECTRA OF DENSE STELLAR WINDS

Dimitri Mihalas and co-workers developed the formalism and the numerical algorithms to model the atmospheres of hot stars in non-LTE. After having accomplished this task for the static, plane-parallel case, the problem of spherically expanding atmospheres was attacked in a series of seminal papers by Mihalas, Kunasz, and Hummer in the years 1975/76.

One important step was to realize that the radiative transfer in highly supersonic flows, where the Doppler shifts are much larger than the width of the line absorption profile, are treated most conveniently in the co-moving frame of reference (CMF). For the equations of statistical equilibrium the "radiative transition rates" are required, and these have to be evaluated with the (angle-averaged) radiation intensity in the CMF as it is "seen" by the matter. As a drawback, the equation of radiative transfer becomes a *partial* differential equation in the CMF: because the frequency  $\nu$  is measured with respect to the co-moving frame, a photon is changing its frequency when propagating through the differentially moving medium. For a ray with coordinate  $z$ , a velocity  $v$  in radial direction, and angle  $\vartheta = \arccos \mu$  between the radial direction and the ray, the CMF transfer is

$$\frac{\partial I_\nu}{\partial z} - \frac{\nu}{c} \frac{d(\mu \nu)}{dz} \frac{\partial I_\nu}{\partial \nu} = \kappa (I_\nu - S_\nu) . \quad (1)$$

In spherically extended atmospheres, the radiation field becomes very anisotropic, and hence many rays of different angle (or, impact parameter) are needed for an accurate numerical representation. However, for isotropic opacity the radiative rates depend only on the angle-averaged radiation intensity  $J_\nu$ . Therefore it is sufficient, and much more economic, to solve the *moment* equations of the radiative transfer. Most of the iterations can be performed by solving the moment equations with given Eddington factors. Only from time to time the latter must be updated. For this purpose the moments of the radiation field must be newly integrated (Eq. (2)) from the angle-dependent intensity, which is obtained from solving the angle-dependent transfer equation for many rays.

As a closure to the moment equations, Auer & Mihalas (1970) introduced the “method of variable Eddington factors” for the static case. In Mihalas, Kunasz & Hummer (1976) they extended this concept to spherically expanding atmospheres. *Four* moments of the radiation intensity are needed in this case:

$$[J_\nu, H_\nu, K_\nu, N_\nu] = \int d\mu I_\nu [1, \mu, \mu^2, \mu^3] . \quad (2)$$

Eddington factors are defined as  $f = K_\nu/J_\nu$  (like in the static case) and  $g = N_\nu/H_\nu$ .

In the numerical application of this method, we encountered problems with both of these definitions. On physical grounds, the intensity-like moment  $J_\nu$  should be positive. Solving the angle-dependent CMF transfer Eq. (1) by means of a Feautrier-like differencing scheme, however, sometimes yields slightly negative values at some frequency and radius points, just due to the limited numerical accuracy. This can make the definition of the Eddington factor  $f = K_\nu/J_\nu$  singular. We overcame this problem by solving the angle-dependent radiative transfer with an *integration* method along short characteristics. Such method can guarantee positive intensities.

The problem with the other Eddington factor,  $g = N_\nu/H_\nu$ , is even more severe. There is actually no reason why the Eddington flux  $H_\nu$  may not become negative in some situations. Therefore we replaced the originally proposed definition of  $g$  by  $g' = N_\nu/J_\nu$ . Although now relating a flux-like to an intensity-like moment, this Eddington factor behaves well in the iteration process.

For the simultaneous solution of the (discretized) radiative transfer equation and the constraint equations, Mihalas and co-workers composed a large system of algebraic equations and solved them by linearization and elimination techniques. Such method is very much restricted to only a few atomic levels and transitions.

Present-day non-LTE codes instead simply solve the radiative transfer and the statistical equilibrium in turn. Such an iteration scheme, a so-called lambda iteration, does not converge when large optical depths are involved. However, in the 1980s it has been discovered that convergence can be achieved when only the local feedback of the radiative transfer is consistently incorporated into the statistical equations. This method, termed “accelerated lambda iteration (ALI)” or “approximate lambda operator (ALO)” technique, allows to calculate model atmospheres with many hundred non-LTE levels, thousands of line transitions, and even millions of further lines in an approximate way as needed for “iron line blanketing” (see Fig. 1 for an example).

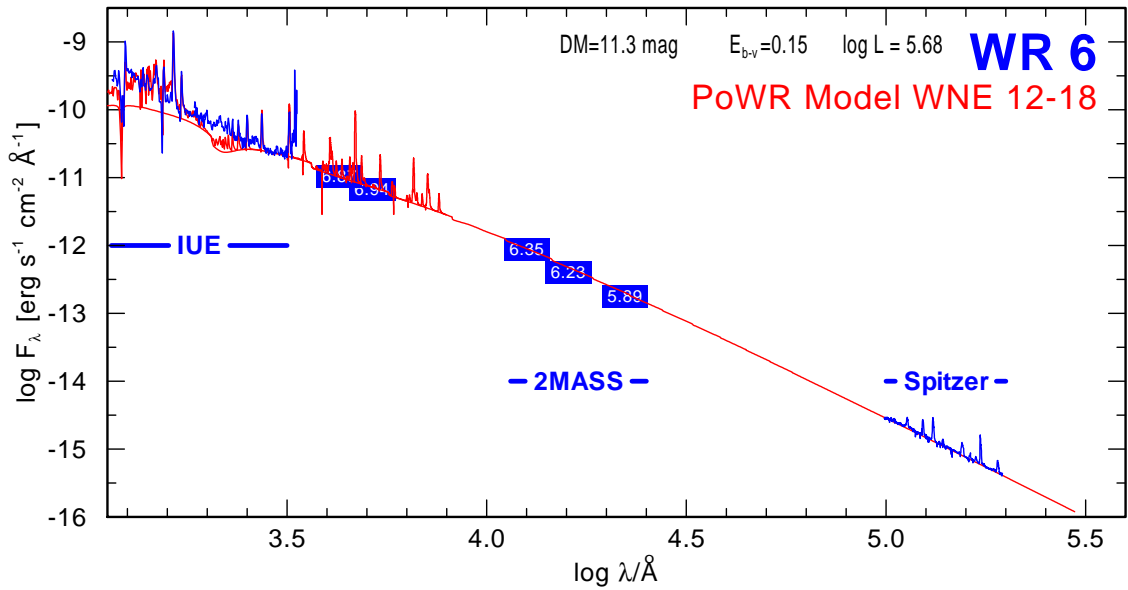


**FIGURE 1.** Observed (blue) spectral energy distribution of the Wolf-Rayet star WR 6 (WN4) from the UV (IUE) to the mid-IR (Spitzer), compared to a Potsdam Wolf-Rayet model (red) from the published grid (<http://www.astro.physik.uni-potsdam.de/PoWR.html>) after applying interstellar reddening.

## 2. STELLAR WINDS HYDRODYNAMICS

### 2.1. Single scattering

Mass-loss from O stars is driven by the momentum transfer from UV photons to the ions of heavy elements. This has been worked out in hydrodynamically self-consistent models for O stars, based on the fundamental concept of Castor, Abbott & Klein (1975). The photospheric radiation is absorbed in a large number of lines, some of them being optically thick. A line which remains optically thick throughout the wind sweeps up all photospheric flux over a bandwidth  $\Delta\nu = \nu_0 v_\infty/c$ , as illustrated in Fig. 2. The intercepted momentum is then  $L_{\nu_0} \Delta\nu/c = L v_\infty/c^2$  where  $L_{\nu_0} = L/\nu_0$  is the specific luminosity at the line frequency  $\nu_0$ . Comparison with the wind momentum per time,  $\dot{M} v_\infty$ , reveals that the mass-loss rate driven by a single optically thick line is  $L/c^2$  – remarkably just the same rate by which mass is converted to energy in the stellar interior for sustaining the luminosity. The actual mass-loss rate in a star can be conveniently expressed in terms of a  $n_{\text{eff}}$ , the effective number of lines:  $\dot{M} = n_{\text{eff}} L/c^2$ . As hydrogen burning consumes about 120 times more fuel than the mass that is converted into energy, wind mass loss becomes a significant driver of stellar evolution when  $n_{\text{eff}}$  is comparable to this factor.

Within this model approach, the maximum mass-loss rate is obviously reached when the whole spectrum is covered by lines and each photospheric photon delivers its momentum once to the wind, i.e. when  $n_{\text{eff}} = c/v_\infty$  or  $\dot{M} = L/(v_\infty c)$ .

The mass-loss rates from O and B stars fall below this “single-scattering limit”, albeit

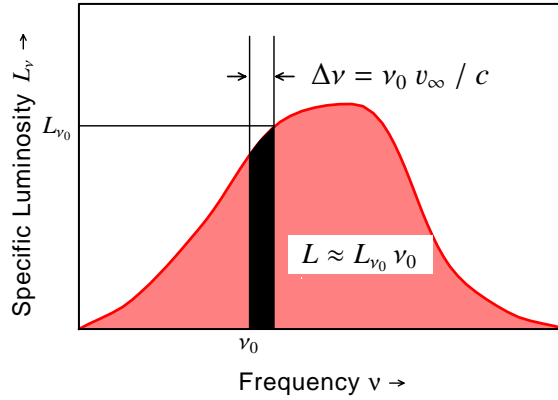


**FIGURE 2.** Absorption by one optically thick wind line at about the maximum of the photospheric flux

for supergiants like  $\zeta$  Pup not by much. For many of the Wolf-Rayet stars, however, empirical mass-loss rates exceed this limit considerably. The CAK models fall short to explain such dense winds.

## 2.2. Multiple scattering

Mass-loss exceeding the single-scattering limit requires that photons deliver their momentum more than once. Such multiple-scattering effects are not included in CAK-type models. To overcome this shortfall, we combined the Potsdam Wolf-Rayet POWR model atmosphere code with the hydrodynamic equations. As the whole radiative transfer is treated consistently, all possible multi-line effects are automatically included. Indeed we obtained self-consistent WR models, as has been demonstrated in Gräfener & Hamann (2005) for the WC5 prototype WR 111. Figure 3 shows for this model how the inward and outward forces are perfectly balanced in the consistent, stationary hydrodynamic solution. Hence we are sure now that the winds of WR stars can be driven by radiation pressure. The previous shortfalls in explaining WR winds were obviously due to deficiencies in the conventional radiative-transfer treatment in CAK-type models.

Specifically in the dense winds from WR stars the multiple-scattering effects from the numerous lines of iron-group elements become important. But why WR stars develop so much denser winds than O stars? We have studied this question by means of a model grid for luminous WN stars of late subtype (WNL) in Gräfener & Hamann (2008). According to our self-consistent HD models, the key point is the  $L/M$  ratio (see Fig. 4). WR stars are just very close to the Eddington limit where the radiation pressure on free electrons balances gravity ( $\Gamma_e = 1$ ). Mass-loss rates of about  $10^{-5} M_\odot/\text{yr}$ , as typical for WR stars, are obtained for an Eddington  $\Gamma_e$  of 0.5 if the metallicity is solar. But even at very low metallicity, strong winds are predicted if  $\Gamma_e$  is sufficiently close to unity.

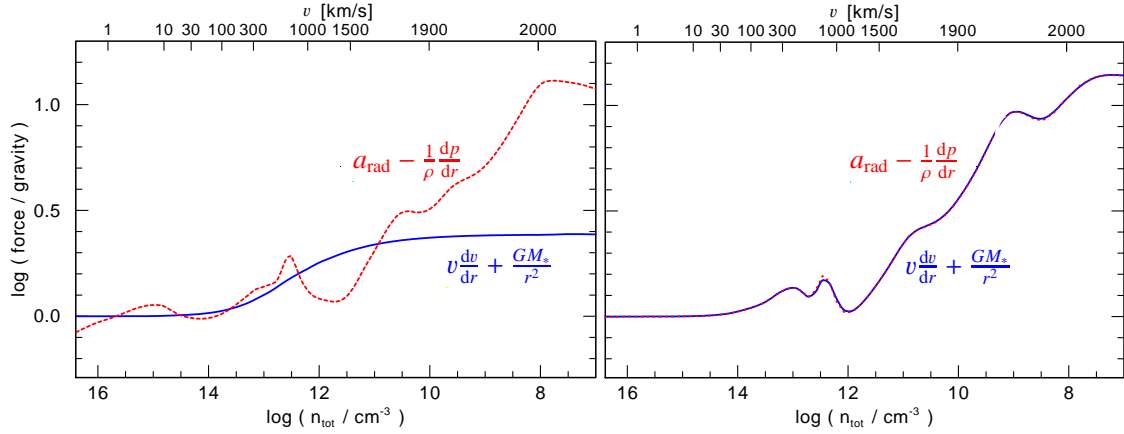


**FIGURE 3.** Acceleration as function of radius (represented by the atomic number density) for a WR wind (model for the WC5 star WR 111, after Gräfener & Hamann 2005). In order to satisfy the hydrodynamic equation, the inward forces (inertia plus gravity, solid/blue line) must be balanced by the outward forces (radiative acceleration  $a_{\text{rad}}$  and pressure gradient, red/dotted curve). For a model with prescribed velocity field (“beta law”) and mass-loss rate, the equality of both terms is not given (left panel). By incorporating the hydrodynamical equations into the PoWR model atmosphere code, a solution for  $\dot{M}$  and  $v(r)$  is found that is hydrodynamically consistent everywhere in the wind (right panel).

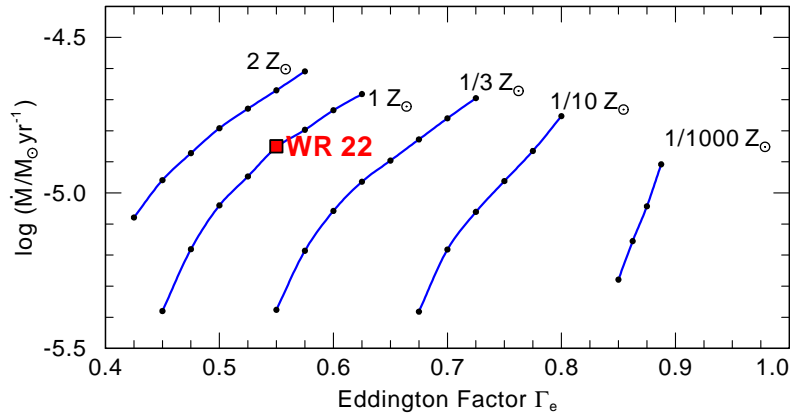


**FIGURE 4.** Mass-loss rates for models of the same luminosity ( $10^{6.3} L_{\odot}$ ), but different  $L/M$  ratio (Eddington factor  $\Gamma$ ) and different metallicities  $Z$  (compared to the solar metallicity  $Z_{\odot}$ ). Hydrodynamically consistent PoWR models are represented by a black dot, blue lines connect models with the same metallicity. The empirical parameters of the WN7 star WR 22 are indicated by a red square. (From Gräfener et al. 2008)

### 2.3. Time-dependent simulations

The hydrodynamic models described in the previous two subsections are stationary solutions of the problem. However, these solutions are expected to be unstable because of the de-shadowing effect: if one volume element would experience a positive perturbation of its velocity, it intercepts more radiation in optically thick lines and is therefore even more accelerated.

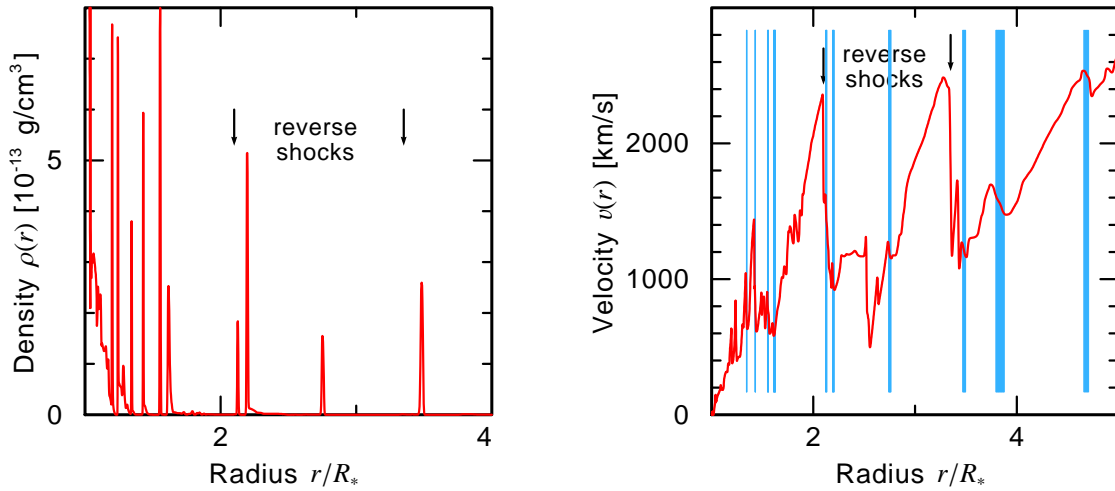


**FIGURE 5.** Snapshot from a 1D-hydrodynamic simulation of a line-driven stellar wind (adapted from Feldmeier et al. 1997). The strong peaks in density (left panel) contain most of the matter. This motivates the *fragmented shell* model of our X-ray studies. The radially compressed shells are created by reverse shocks characterized by strong velocity jumps (right panel). The shaded stripes in the velocity plot indicate the location and radial extension of the overdense shells.

The effect of this instability can be seen in the time-dependent hydrodynamical simulations presented by Feldmeier et al. (1997). These calculations are for spherical symmetry, but account for heating and cooling processes. A snapshot for an O star wind is shown in Fig. 5. The instability leads to the formation of dense shells, which contain almost all of the wind material and have a radial separation of about one stellar radius. These structures are created by strong reverse shocks with velocity jumps of several hundred km/s. The shocked gas reaches temperatures of a few million Kelvin.

Corresponding multidimensional simulations which account for the radiative force on lines in non-radial directions and for the heating and cooling of the shocks are not yet available.

### 3. INHOMOGENEOUS STELLAR WINDS

#### 3.1. Microclumping

As discussed in Sect. 2.3, hot-star winds are expected to be structured by the hydrodynamic instability that is inherent to the line-driving mechanism. This prediction is supported by various observational evidences for wind variability and inhomogeneity. An important spectroscopic fingerprint of wind “clumping” had been pointed out already by Hillier (1984), namely the electron-scattering wings of strong emission lines. The “Thomson scattering” of photons by free electrons is often considered as being coherent. However, this is only correct in the rest frame of the electron (when neglecting the Compton shift due to the recoil), but not when considering the electron’s thermal motion. In fact, the thermal speed of the electrons is very high, about 500 km/s at 10 kK,

and therefore the corresponding Doppler shift causes a redistribution in frequency that is comparable with the width of wind-broadened emission lines.

The emission lines that dominate the spectra of Wolf-Rayet stars are mainly fed by recombination cascades. The recombination process scales with the square of the density. The Thomson scattering, in contrast, scales linearly with the (electron) density. Considering an inhomogeneous medium, the ratio between the mean of the density-squared and the square of the mean density,  $\langle \rho^2 \rangle / \langle \rho \rangle^2$ , becomes larger than unity. Therefore, the fit of emission lines and their electron-scattering winds can provide a tool to estimate the degree of stellar-wind clumping.

In a simple approach, one can assume that the whole stellar wind is concentrated in clumps, while the interclump medium is void. When the clumps fill a fraction  $f_V$  of the volume, the density in the clumps is by a factor  $D = f_V^{-1}$  enhanced over a smooth wind.

A further simplifying assumption is that the individual clumps are optically thin at all frequencies. This approximation is termed “microclumping”. It can be easily implemented in model atmosphere codes, as it leaves the radiation field homogeneous. For Wolf-Rayet stars, the electron-scattering wings of strong emission lines are usually well reproduced with this formalism when the clumping contrast  $D$  is set to values between 4 and 10 (e.g. Hamann & Koesterke 1998). The spectra of O and B stars, however, do not show strong enough emission lines for which this method could be applied. There are empirical indications that clumping develops already deep in the wind where the expansion velocity is still small, and decreases at larger distance from the star (Puls et al. 2006).

A major consequence of microclumping is a reduction of empirical mass-loss rates that are derived from  $\rho^2$ -depending processes, such as emission lines fed by recombination cascades, as well as the free-free radio emission. Compared to “unclumped” diagnostic, this reduction is by a factor of  $\sqrt{D}$ .

In a recent work, Zsargó et al. (2008) introduced a second, diluted wind component that fills the space between the clumps. This thin interclump gas becomes more easily ionized, especially from hard radiation produced in wind shocks, and therefore contributes to the spectral lines from high ions, e.g., from O VI.

## 3.2. Macroclumping

The *microclumping* assumption that the individual clumps have only small optical depth cannot be justified for all frequencies. The wind-compressed shells in the hydrodynamical simulations (cf. Fig. 5) have a thickness of the order of  $0.1 R_*$ . Estimates from variability lead to similar clump diameters. In the winds from WR and O-type stars, clumps of such size are expected to be optically thick in the cores of strong lines, and also in the far-UV and soft X-ray continua from bound-free and K-shell absorption. Therefore we introduce a more general concept which accounts for the finite optical thickness of clumps. However, drastic approximations are necessary to keep the problem manageable.

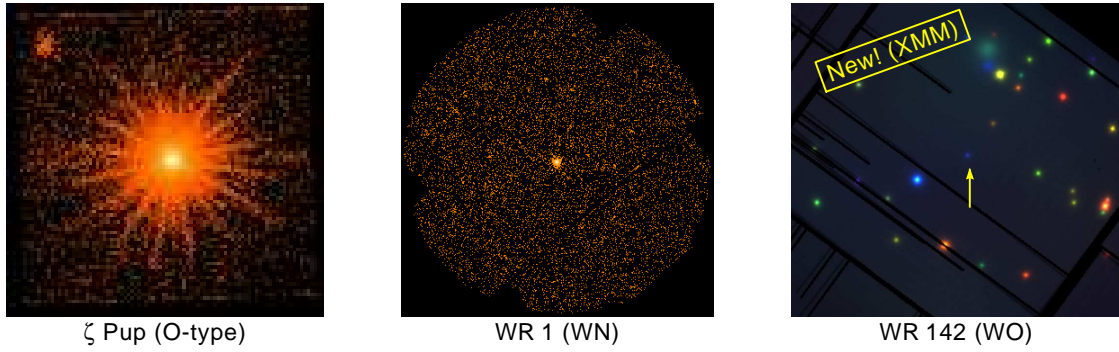


**FIGURE 6.** Illustration of the different X-ray brightness of stellar winds. While O-star winds are often strong X-ray sources, only some of the WN stars show a measurable X-ray flux, when all binaries are disregarded. As the first, albeit faint X-ray source among the WO/WC class, we recently detected the very hot and compact WO star WR 142.

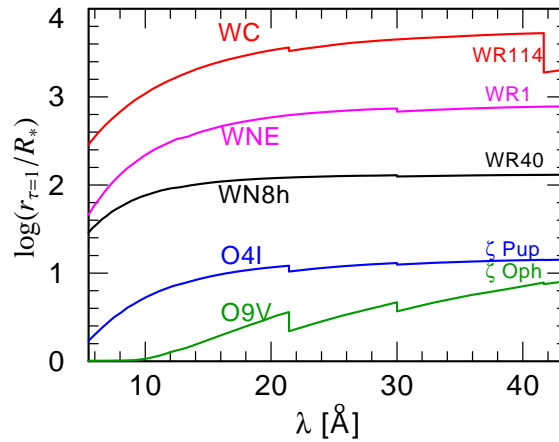


**FIGURE 7.** Radius where the radial optical depth reaches unity, plotted versus wavelength in the X-ray range. The high continuum opacity is due to bound-free and K-shell absorption. The models are for typical parameters, but without clumping.

### 3.2.1. Macroclumping and X-rays

Early-type stars can be often observed as X-ray sources. Many such sources are found to be binaries, where the X-rays may be produced by the collision of two stellar winds. However, there are also many putatively single early-type stars with X-ray detections.

X-ray emission is believed to originate from hot, shocked gas embedded in the stellar winds. There are two arguments why the X-rays are production must be located in the inner wind region, firstly because the line-driving instability should be largest where the acceleration is strongest, and secondly because the X-ray line profiles are typically wind-broadened with only about half of the terminal wind velocity. In order to be observable, this X-ray emission has to escape from the expanding atmosphere through the absorbing “cool” wind component which contains the bulk of the matter. This wind attenuation may account for the observed decrease of the emergent X-ray flux with increasing

density of the stellar wind illustrated in Fig. 6.

Checking this wind attenuation quantitatively reveals a severe problem, as demonstrated in Fig. 7. For X-ray wavelengths where emission lines are observed, the plot shows the radius where the radial optical depth reaches unity. According to these predictions from typical models, X-rays should not be able to escape from lower wind regions, at least not for an O supergiant like  $\zeta$  Pup, and definitely not for Wolf-Rayet stars.

An escape from this dilemma can be searched by reducing the stellar mass-loss rates by adopting very high clumping factors  $D$ . At least in the case of WN stars this runs in various contradictions, e.g. with the electron-scattering line wings (see above), or with the mass-loss rate of the binary V444 Cyg from its period change.

Alternatively, we have shown that the X-ray observations can be explained when the macroscopic size of the clumps is taken into account. The X-rays lines are emitted from hot shocks, while the absorption takes place in the cool wind component by continuum processes. This decoupling of emission and absorption greatly facilitates a semi-empirical modeling.

Monte-Carlo calculations have been applied to model the emergent X-ray line profiles with randomly distributed line emitters and absorbing clumps (Oskinova et al. 2004, 2006). Basically the same results are obtained from an analytical treatment that holds in the limit that the emitting spots and the absorbing clumps are numerous enough for a statistical description (Feldmeier et al. 2003, Owocki & Cohen 2006). The consequence of the wind clumping is a reduction of the effective opacity. Some atomic absorbers are hiding in the shadow of others, while the gaps between the shell fragments open channels where photons can travel far.

The Potsdam work (Feldmeier et al. 2003, Oskinova et al. 2004, 2006) found that the observed X-ray line profiles can be explained best if the “clumps” are assumed to have the shape of “pancakes” or “shell fragments” (see Fig. 8). This idea is also supported from the theoretical consideration that the forces which compress the clumps act mainly in radial direction. If clumps are anisotropic, their *projected* cross section leads to a “venetian blind effect”, where in the limit of entirely flat fragments the opacity scales proportional to  $\mu = \cos \vartheta$ . With the corresponding effective opacity becoming angle-dependent as  $\kappa_{\text{eff}} \propto \mu$ , the optical depth increment for a ray of any impact parameter grows with the change of radius:  $d\tau \propto |dr|$ , in contrast to the isotropic case where  $d\tau = \kappa dz$ .

### 3.2.2. Macroclumping and line formation

In Oskinova et al. (2007) we considered specifically the case of a spectral *line* formation. We take the statistical approach as already used for the X-ray absorption, but in the line case we restrict ourselves to isotropic clumps which have the same optical diameter  $\tau_{\text{clump}}$  in all directions. At a given location, all clumps have uniform size. Under these assumptions, the *effective* opacity becomes

$$\kappa_{\text{eff}} = h^{-1} (1 - e^{-\tau_{\text{clump}}}) = \kappa_{\text{smooth}} \frac{1 - e^{-\tau_{\text{clump}}}}{\tau_{\text{clump}}} \quad (3)$$

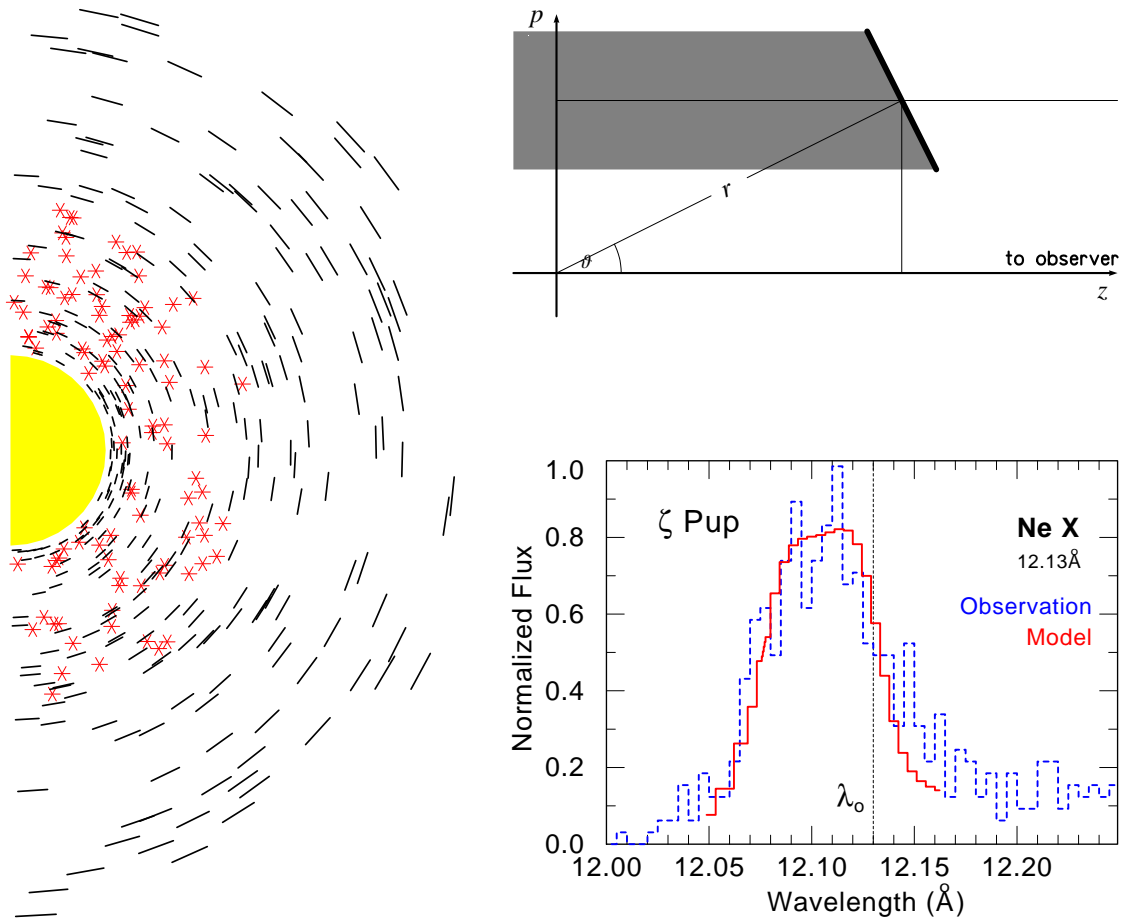


**FIGURE 8.** The *fragmented shell model* for the formation of X-ray lines. The radiation is emitted from randomly distributed shocks (red stars in the left sketch) and absorbed by radially compressed shell fragments. In the radiative transfer calculations, these fragments are treated as thin slabs, leading to an angle-dependent opacity (see upper-right sketch). Only with these assumptions the model (red) can reproduce the shifted and skewed X-ray line profiles as observed (blue-dashed).

where  $h$  is the well-known “porosity length” (e.g. Owocki, Gayley & Shaviv 2004). Note that for optically thin clumps the smooth-wind opacity  $\kappa_{\text{smooth}}$  is recovered, while in the limit of large  $\tau_{\text{clump}}$  the effective opacity becomes  $\kappa_{\text{eff}} = h^{-1}$ .

In the case of line formation we have to address the issue of Doppler shifts. In our one-component model *the clumps are the wind*. Hence clumps as such move with the wind velocity field  $v(r)$ . Due to the supersonic expansion, rays of a given (observer’s frame) frequency can only interact with clumps near the *surface of constant radial velocity* (CRVS). The line opacity of all other clumps is Doppler-shifted out of the resonance. Hence the porosity effect for lines is very pronounced, as illustrated in Fig. 9.

An important issue is the Doppler broadening *within* a clump, which widens the CRVS to a resonance *zone*. We describe the clump opacity with a gaussian distribution corresponding to a Doppler-broadening velocity  $v_D$ , which may schematically account for the velocity distribution inside the clump caused by stochastic motion (thermal,

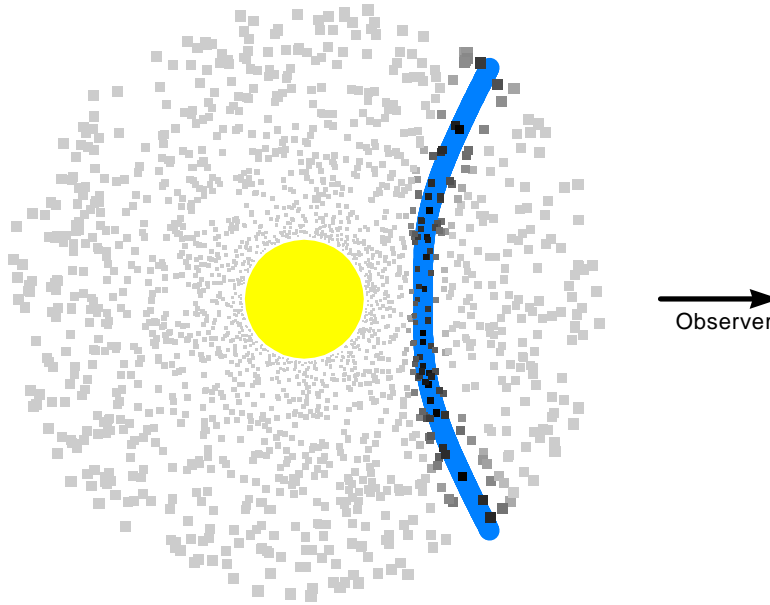


**FIGURE 9.** Porosity in the case of line opacity. At a given observer’s frame frequency, rays can only interact with those clumps (dark shaded) that are close to the *constant radial velocity surface* (CRVS, blue thick curve), while other clumps (light grey) are out of the line resonance.

microturbulent), as well as by velocity gradients. Note that the degree of porosity for line radiation depends on this parameter: for smaller  $v_D$ , the opacity profile of a clump peaks to a higher maximum, resulting in a smaller effective opacity of the atmosphere.

The 1D hydrodynamic calculations shown in Fig. 5 predict that within the dense shells the radial velocity gradient is negative, and span typically over a velocity range of 100 km/s or less. When the motion is strictly radial, the transverse velocity gradient is positive. Assuming that the clumps cover a cone angle of a few degrees (seen from the center of the star), a wind speed of  $\approx 2000$  km/s leads to a transverse expansion of a clump with less than 100 km/s.

Empirically it is known that the narrowest spectral features from stellar winds, like the DACs (discrete absorption components), still have typical widths corresponding to 50 ... 100 km/s. Therefore values of  $v_D$  in this range seem to be a reasonable choice.

A further important parameter is of course the clump size, which is related to the mean separation of the clumps, and to their total number at one instant of time. Several observational and theoretical arguments help to restrict this parameter, as discussed in Oskinova et al. (2007). There we implemented the *macroclumping* formalism only in the “formal integral” of the PoWR code, thus making the first approximation that the non-LTE source function is not affected.

A motivation of this study was the so-called P v problem. Bouret et al. (2005) and Fullerton et al. (2006) had pointed out that in O star spectra the P v resonance line in the extreme UV is observed much weaker than predicted. They suggest to reduce drastically the adopted mass-loss rates, and compensate for this by higher density-enhancement factors  $D$  in the microclumping treatment. Resonance lines depend, like the electron-scattering wings discussed in Sect. 3.1, only linearly on density.

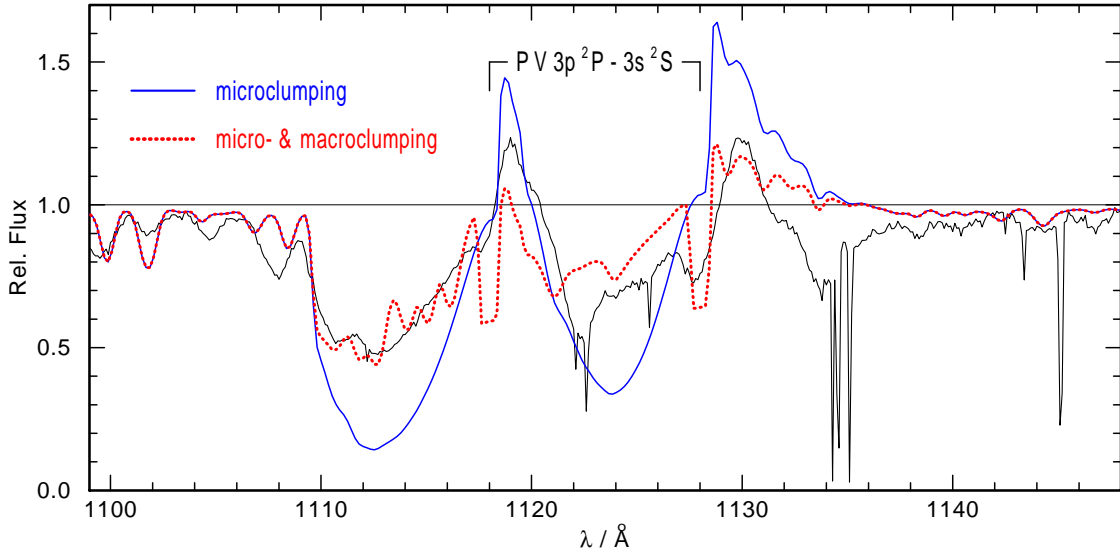


**FIGURE 10.** Effect of macroclumping on the P v resonance doublet at 1118/1128 Å for an O star. The spectrum of  $\zeta$  Pup as observed by COPERNICUS is shown for comparison (black, ragged line). We adopt a microturbulence velocity of 50 km/s to account for the velocity dispersion inside the clumps. Numerous weak spectral features in this range are due to iron. The usual modeling yields much too strong P Cygni features (blue, continuous line). With our macroclumping formalism, the line features are reduced to the observed strength (red, dotted curve). From Oskinova et al. (2007)

In Oskinova et al. (2007) we have shown that the macroclumping formalism can explain the weakness of the P v resonance line without a further reduction of the mass-loss rate (see Fig. 10).

As an unwanted side effect, macroclumping slightly de-saturates the black absorptions of strong UV resonance lines like the doublets from C IV and N v. However, according to Zsargó et al. (2008) these lines are anyhow not mainly formed in the dense clumps, but in the diluted interclump medium which is neglected in our modeling.

## REFERENCES

1. Auer, L.H., Mihalas, D. 1970, MNRAS, 149, 65
2. Castor, J.I., Abbott, D.C., & Klein, R. 1975, ApJ, 195, 157
3. Feldmeier, A., Oskinova, L. M., & Hamann, W.-R. 2003, A&A, 403, 217
4. Feldmeier, A., Kudritzki, R. P., Palsa, R., Pauldrach, A. W. A., & Puls, J. 1997, A&A, 320, 899
5. Gräfener, G., & Hamann, W.-R. 2005, A&A, 432, 633
6. Gräfener, G., & Hamann, W.-R. 2008, A&A, 482, 945
7. Hamann, W.-R., Koesterke, L. 1998, A&A, 335, 1003
8. Hillier, D.J. 1984, ApJ, 280, 744
9. Mihalas, D., Kunasz, P.B., Hummer, D.G. 1976, ApJ, 210, 419
10. Oskinova, L. M., Feldmeier, A., & Hamann, W.-R. 2004, A&A, 422, 675
11. Oskinova, L. M., Feldmeier, A., & Hamann, W.-R. 2006, MNRAS, 372, 313
12. Oskinova, L. M., Feldmeier, A., & Hamann, W.-R. 2007, A&A, 476, 1331
13. Owocki, S. P., & Cohen, D. H. 2006, ApJ, 648, 565
14. Puls, J., Markova, N., Scuderi, S., et al. 2006, A&A, 454, 625
15. Zsargó, J., Hillier, D.J., Bouret, J.-C., et al. 2008, ApJ, 685, 149